Acta Mech 233, 4029–4046 (2022)
https://doi.org/10.1007/s00707-022-03318-z

ORIGINAL PAPER

H. T. Wang · J. H. Guo · X. Jiang · M. Z. Gao

Bending and vibration of one-dimensional hexagonal quasicrystal layered plates with imperfect interface

Received: 26 March 2022 / Revised: 16 July 2022 / Accepted: 29 July 2022 / Published online: 30 August 2022

Abstract In this paper, the bending deformation, free vibration and forced vibration of one-dimensional hexagonal quasicrystal layered plates with imperfect interfaces are investigated. The generalized linear spring layer model is adopted to simulate the interface bonding defects caused by the slip or debonding of quasicrystal materials due to actual production or interlayer aging. The imperfect interface transfer matrix is established for one-dimensional hexagonal quasicrystal layered plates and the analytical solutions of phonon displacements, phonon stresses, phason displacements and phason stresses for static bending, the natural frequency for free vibration, and the displacements of phonon and phason fields for forced vibration under a harmonic excitation are then derived by the pseudo-Stroh formalism. Numerical examples are provided to analyze the influence of the stacking sequence and the imperfect interface parameter of two sandwich plates composed of crystal and quasicrystal materials on the bending deformation and vibrational response of layered quasicrystal composite plates. Furthermore, the presented three-dimensional plate model is applied to quasicrystal-coated aluminium-based composites in engineering practice.

1 Introduction

Quasicrystals (QCs) have many excellent properties such as high strength, corrosion resistance, low thermal conductivity, low adhesion and low level of porosity due to their quasiperiodic structures [1]. Different from ordinary crystal materials, there are two elementary excitations, i.e., phonon and phason, in the study of QCs based on the Landau phenomenological theory [2]. The former describes the classical motion of atoms in crystals, whereas the latter corresponds to the spatial rearrangement of atoms [3]. However, QCs are brittle at room temperature, which limits their application as structural components in engineering. Thus, QCs are commonly used as surface coatings and reinforcement phases of composites to enhance the mechanical properties of soft metal matrices and alloys [4–6].

H. T. Wang · J. H. Guo (✉)
Department of Mechanics, Inner Mongolia University of Technology, Hohhot 010051, People's Republic of China
e-mail: jhguo@imut.edu.cn

H. T. Wang
e-mail: tcgkwht@163.com

J. H. Guo
School of Aeronautics, Inner Mongolia University of Technology, Hohhot 010051, People's Republic of China

X. Jiang (✉) · M. Z. Gao
College of Energy and Power Engineering, Inner Mongolia University of Technology, Hohhot 010051, People's Republic of China
e-mail: jiangxin@imut.edu.cn

M. Z. Gao
e-mail: 664136612@qq.com

A layered plate or laminate as an important composite structure has the advantages of small specific gravity, large specific strength and specific modulus. Duguet et al. [7] demonstrated the possibility of using complex metallic surface alloys as interface layers to enhance the adhesion between QCs and simple metal substrates. Chang et al. [8] formed multilayered coatings by ductile vanadium layers and brittle Al-Cu-Fe-based QC layers and found that the annealed multilayered structure showed a high flow stress due to QC strengthening. Ali et al. [9] investigated the interfacial reaction between Al matrix and QC reinforcing particles to enhance the strength of the Al/QC composites. By using a facile method of heat treatment, Wei and He [10] synthesized a multilayered sandwich-like three-dimensional (3D) structure containing large-scale faceted Al-Cu-Fe QC grains. The pseudo-Stroh formalism is an effective method to obtain the exact solutions for a simply supported and multilayered QC plates. For example, by using the pseudo-Stroh formalism, Yang et al. [11, 12] derived exact solutions for one-dimensional (1D) orthorhombic and two-dimensional (2D) decagonal QC multilayered plates. Waksmanski et al. [13] addressed an exact closed-form solution of free vibration of a simply-supported and multilayered 1D QC plate. With the rapid development of nanotechnology and advanced materials, the mechanical behaviors of multilayered QC nanoplates have been widely investigated. Pan and Waksmanski [14] presented an exact closed-form solution for the 3D static deformation and free vibrational response of a simply-supported and multilayered QC nanoplate with nonlocal effect. Based on the modified couple-stress theory, Li et al. [15] analyzed the static bending deformation of multilayered 1D hexagonal QC nanoplates under surface loadings. Furthermore, Guo et al. [16] investigated the free and forced vibration of layered 1D QC nanoplates with modified couple-stress effect. Recently, the nonlocal strain gradient theory was adopted to investigate the static bending deformation of a functionally graded multilayered nanoplate made of 1D hexagonal piezoelectric QC materials subjected to mechanical and electrical surface loadings [17]. For the other boundary conditions, it is difficult to obtain the general solutions of layered structures by using the pseudo-Stroh formalism. More recently, the state space and differential quadrature approach was adopted to solve the free vibration and bending of 1D QC layered composite beams with various boundary conditions [18].

Most of the previous work mentioned above on multilayered plates is based on the assumption that all the interfaces between different layers are perfect bonding. In other words, the extended displacement and stress are continuous across the interfaces of layered plates. However, due to manufacturing or interlaminar aging and other reasons, microcracks or cavities may occur at the interfaces, which could lead to interface slip or debonding. Cheng et al. [19, 20] presented a linear theory underlying elastostatics and kinetics of multilayered anisotropic plates and laminated shells with imperfect interfaces. This theory has the same advantages as conventional higher-order theories over the classical and the first-order theories. Based on the self-consistent scheme, Fan and Sze [21] proposed a micro-mechanical model to account for the imperfect interface in dielectric materials. Bui et al. [22] used the interface finite elements to investigate the effects of imperfect interlaminar interfaces on the overall mechanical behavior of composite laminates. This numerical approach is an efficient tool for treating laminated composite structures with complicated geometry and/or loading. The state space method and the extended pseud-Stroh formalism are employed to obtain the exact solutions of 3D anisotropic elasticity, which canaccurately predict the mechanical behaviors of thick plates. Chen et al. [23, 24] analyzed the bending and free vibration of a simply-supported, cross-ply laminated rectangular plate featuring interlaminar bonding imperfections. Wang and Pan [25] derived 3D exact solutions for simply-supported and multilayered rectangular plates with imperfect interfaces under static thermo-electro-mechanical loadings. Chen et al. [26] used the state space formulations to consider the bending problem of a multiferroic rectangular plate with magnetoelectric coupling and imperfect interfaces. Based on the extended pseud-Stroh formalism and the dual variable and position method, Kuo et al. [27] derived analytical solutions of static bending for a simply supported, anisotropic and multilayered magneto-electro-elastic plate with imperfect interfaces. Recently, Vattré and Pan [28] derived 3D exact solutions of temperature and thermoelastic stresses in multilayer anisotropic plates and free vibration of fully coupled thermoelastic multilayered composites with imperfect interfaces. Besides, López-Realpozo et al. [29] used the two scales asymptotic homogenization method to determine the effective coefficients of laminated piezoelectric composite with periodic structure under nonuniform electrical and mechanical imperfect contact conditions. The meshless method has the advantage in the field of computational mechanics over the above methods. For instance, a regularized method of moments and the modified multilevel algorithm proposed by Li et al. [30–32] show the high precision, the reduction of computational time and the rapid iteration in the calculation, etc.

However, no work on the static deformation and vibrational response of 1D hexagonal layered QC plates with imperfect interfaces has been reported so far. Therefore, this paper focuses on the static bending, free vibration and forced vibration of 1D hexagonal layered QC plates with imperfect interfaces. Exact solutions of

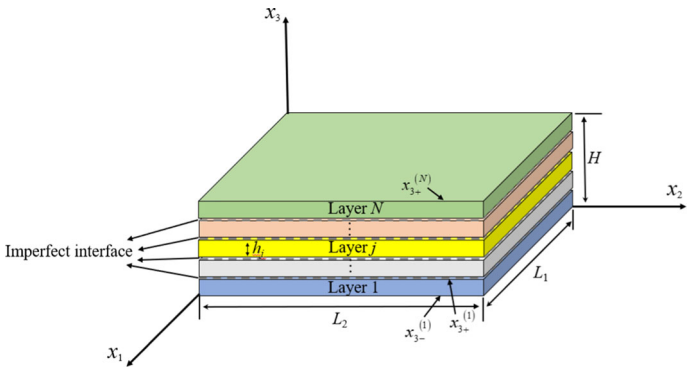

Fig. 1 An N-layer QC plate with imperfect interfaces

the extended stress and displacement (displacements and stresses of phonon and phason fields) of multilayered QC plates are derived by the propagation matrix method and pseudo-Stroh formulism. The effect of imperfect interface parameter and stacking sequence on the static deformation and vibrational response of two sandwich plates made up of crystal and QC materials is analyzed in the numerical examples.

2 Problem description and basic equations

According to the quasiperiodic directions of QCs, there are three kinds of QCs which are classified as 1D, 2D and 3D QCs [2]. The 1D QCs considered in this work are in a 3D structure in which its atomic arrangement is quasi-periodic in one direction and periodic in the plane perpendicular to that direction. We consider an anisotropic and N-layer rectangular 1D hexagonal QC plates with imperfect interfaces, with horizontal dimensions L_1 and L_2 and total thickness H, and its four sides being simply supported. As shown in Fig. 1, the Cartesian coordinate system (x, y, z) corresponds to (x_1, x_2, x_3) in the figure, and the positive x_3-direction is along the thickness of the plate. The quasi-periodic direction is along the positive x_3-axis direction. For any layer j $(1 \le j \le N)$, layer j is bonded by its lower interface $x_{3-}^{(j)}$ and upper interface $x_{3+}^{(j)}$ such that its thickness is $h_j = x_{3+}^{(j)} - x_{3-}^{(j)}$ and $H = h_1 + h_2 + \ldots + h_N$, where + and − represent the upper and lower surfaces of each interface, respectively. It is assumed that the interface between two layers is imperfect or has some defects due to improper preparation or use. Based on the linear elastic theory of 1D QCs, the basic equations include [1]

$$\begin{aligned}
\sigma_{11} &= C_{11}\varepsilon_{11} + C_{12}\varepsilon_{22} + C_{13}\varepsilon_{33} + R_1\omega_{33},\\
\sigma_{22} &= C_{12}\varepsilon_{11} + C_{11}\varepsilon_{22} + C_{13}\varepsilon_{33} + R_1\omega_{33},\\
\sigma_{33} &= C_{13}\varepsilon_{11} + C_{13}\varepsilon_{22} + C_{33}\varepsilon_{33} + R_2\omega_{33},\\
\sigma_{23} &= \sigma_{32} = 2C_{44}\varepsilon_{23} + R_3\omega_{32},\\
\sigma_{31} &= \sigma_{13} = 2C_{44}\varepsilon_{31} + R_3\omega_{31},\\
\sigma_{12} &= 2C_{66}\varepsilon_{12},\\
H_{31} &= 2R_3\varepsilon_{31} + K_2\omega_{31},\\
H_{32} &= 2R_3\varepsilon_{23} + K_2\omega_{32},\\
H_{33} &= R_1(\varepsilon_{11} + \varepsilon_{22}) + R_2\varepsilon_{33} + K_1\omega_{33},
\end{aligned} \tag{1}$$

$$\begin{aligned}
\sigma_{ij,i} &= \rho\frac{\partial^2 u_i}{\partial t^2},\\
H_{3j,j} &= \rho\frac{\partial^2 w_3}{\partial t^2},
\end{aligned} \tag{2}$$

$$\varepsilon_{ij} = \frac{1}{2}(u_{i,j} + u_{j,i}), \quad \omega_{3j} = w_{3,j}, \quad i,\ j = 1,\ 2,\ 3 \tag{3}$$

In Eqs. (1)–(3), a comma denotes differentiation with respect to x_i $(i = 1, 2, 3)$, repeated indices imply summation. σ_{ij}, ε_{ij} and u_i are the components of the stress, strain and displacement of the phonon field, respectively; H_{3j}, ω_{3j} and w_3 are the components of the stress, strain and displacement of the phason field, respectively; C_{ij}

and K_i are the elastic constants of phonon and phason fields, respectively; R_i are the phonon–phason coupling elastic constants.

Furthermore, the simply-supported boundary conditions can be written as

$$\begin{aligned} x_1 = 0,\ x_1 = L_1: &\quad u_2 = u_3 = w_3 = \sigma_{11} = 0, \\ x_2 = 0,\ x_2 = L_2: &\quad u_1 = u_3 = w_3 = \sigma_{22} = 0. \end{aligned} \tag{4}$$

Due to improper preparation or use of layers, the layered composite structures cannot be perfectly bonded, which results in delamination or slip phenomenon at interfaces [33]. Two imperfect and realistic interface models, i.e., the generalized interface stress type and generalized linear spring type models, are commonly used to simulate the discontinuities of field quantities at interfaces [34–37]. In the former, the stress field is discontinuous while the displacement field is continuous across the interface. In the latter, the displacement field is discontinuous but the stress field is continuous at the interface. In the current work, the generalized linear spring type model is selected to study the static 3D deformation of layered QC composite plate. Thus, for the imperfect interfaces of QCs, we have the following boundary conditions at the interfaces [26]:

$$\begin{aligned} \sigma_{13}^{(j+1)} &= \sigma_{13}^{(j)} = \left[u_1^{(j+1)} - u_1^{(j)}\right]/R_1^{(j)}, \\ \sigma_{23}^{(j+1)} &= \sigma_{23}^{(j)} = \left[u_2^{(j+1)} - u_2^{(j)}\right]/R_2^{(j)}, \\ \sigma_{33}^{(j+1)} &= \sigma_{33}^{(j)} = \left[u_3^{(j+1)} - u_3^{(j)}\right]/R_3^{(j)}, \\ H_{33}^{(j+1)} &= H_{33}^{(j)} = \left[w_3^{(j+1)} - w_3^{(j)}\right]/R_4^{(j)}, \end{aligned} \tag{5}$$

where $R_i^{(j)} (i = 1 \sim 4)$ are the imperfect interface parameters. Equation (5) can be also expressed in matrix form as

$$\begin{bmatrix} \mathbf{u}\left(x_{3-}^{(j+1)}\right) \\ \mathbf{t}\left(x_{3-}^{(j+1)}\right) \end{bmatrix} = \mathbf{M}_j \begin{bmatrix} \mathbf{u}\left(x_{3+}^{(j)}\right) \\ \mathbf{t}\left(x_{3+}^{(j)}\right) \end{bmatrix}, \tag{6}$$

where $\mathbf{u} = [u_1, u_2, u_3, w_3]^T$ and $\mathbf{t} = [\sigma_{13}, \sigma_{23}, \sigma_{33}, H_{33}]^T$ represent the generalized displacement and stress of layer j, respectively, where the superscript T denotes the transpose of a vector or matrix, and the imperfect interface propagator matrix $\mathbf{M}_j$ is given as

$$\mathbf{M}_j = \begin{bmatrix} 1 & 0 & 0 & 0 & \overline{R}_1^{(j)} & 0 & 0 & 0 \\ 0 & 1 & 0 & 0 & 0 & \overline{R}_2^{(j)} & 0 & 0 \\ 0 & 0 & 1 & 0 & 0 & 0 & \overline{R}_3^{(j)} & 0 \\ 0 & 0 & 0 & 1 & 0 & 0 & 0 & \overline{R}_4^{(j)} \\ 0 & 0 & 0 & 0 & 1 & 0 & 0 & 0 \\ 0 & 0 & 0 & 0 & 0 & 1 & 0 & 0 \\ 0 & 0 & 0 & 0 & 0 & 0 & 1 & 0 \\ 0 & 0 & 0 & 0 & 0 & 0 & 0 & 1 \end{bmatrix}, \tag{7}$$

where

$$\overline{R}_i^{(j)} = \frac{R_i^{(j)} H}{C_{44}}, \quad (i = 1,\ 2,\ 3),\quad \overline{R}_4^{(j)} = \frac{R_4^{(j)} H}{K_2}. \tag{8}$$

If $R_i^{(j)}$ is zero, $\mathbf{M}_j$ become the identity matrices. Thus, all the interfaces of QC layered plates become perfect ones. In general, it is assumed that $R_3^{(j)} = 0$ to avoid the impossible phenomenon of material interpenetration [33].

3 Analytical solutions

For a homogeneous 1D hexagonal QC plate with simply-supported on its four sides, the general solution of the extended displacement vector **u** under time-dependent harmonic motion can be expressed as [12, 38]

$$\mathbf{u} \equiv \begin{bmatrix} u_1 \\ u_2 \\ u_3 \\ w_3 \end{bmatrix} = \mathrm{e}^{sx_3+\mathrm{i}\omega t} \begin{bmatrix} a_1 \cos(px_1)\sin(qx_2) \\ a_2 \sin(px_1)\cos(qx_2) \\ a_3 \sin(px_1)\sin(qx_2) \\ a_4 \sin(px_1)\sin(qx_2) \end{bmatrix}, \tag{9}$$

where $p = n\pi/L_1$, $q = m\pi/L_2$, s the eigenvalue to be determined, ω being the angular frequency, imaginary $\mathrm{i} = \sqrt{-1}$, n and m are two positive integers, and $a_1 \sim a_4$ are unknown constants to be determined. By taking the summation over all values of n and m we can derive the general solution in terms of 2D Fourier series expansions.

Then, we can assume the extended stress vector as follows:

$$\mathbf{t} \equiv \begin{bmatrix} \sigma_{13} \\ \sigma_{23} \\ \sigma_{33} \\ H_{33} \end{bmatrix} = \mathrm{e}^{sx_3+\mathrm{i}\omega t} \begin{bmatrix} b_1 \cos(px_1)\sin(qx_2) \\ b_2 \sin(px_1)\cos(qx_2) \\ b_3 \sin(px_1)\sin(qx_2) \\ b_4 \sin(px_1)\sin(qx_2) \end{bmatrix}. \tag{10}$$

According to the constitution equations, the relationship between vector $\mathbf{b} = [b_1, b_2, b_3, b_4]^T$ and vector $\mathbf{a} = [a_1, a_2, a_3, a_4]^T$ yields

$$\mathbf{b} = \left(-\mathbf{R}^T + s\mathbf{T}\right)\mathbf{a} = -\frac{1}{s}(\mathbf{Q} + s\mathbf{R})\mathbf{a}, \tag{11}$$

where

$$\mathbf{R} = \begin{bmatrix} 0 & 0 & C_{13}p & R_1 p \\ 0 & 0 & C_{13}q & R_1 q \\ -C_{44}p & -C_{44}q & 0 & 0 \\ -R_3 p & -R_3 q & 0 & 0 \end{bmatrix}, \quad \mathbf{T} = \begin{bmatrix} C_{44} & 0 & 0 & 0 \\ 0 & C_{44} & 0 & 0 \\ 0 & 0 & C_{33} & R_2 \\ 0 & 0 & R_2 & K_1 \end{bmatrix}, \tag{12}$$

$$\mathbf{Q} = \begin{bmatrix} -C_{11}p^2 - C_{66}q^2 + \rho\omega^2 & -pq(C_{12}+C_{66}) & 0 & 0 \\ -pq(C_{12}+C_{66}) & -C_{66}p^2 - C_{11}q^2 + \rho\omega^2 & 0 & 0 \\ 0 & 0 & -C_{44}(q^2+p^2) + \rho\omega^2 & -R_3(q^2+p^2) \\ 0 & 0 & -R_3(p^2+q^2) & -K_2(p^2+q^2) + \rho\omega^2 \end{bmatrix}. \tag{13}$$

Substituting Eqs. (9) and (10) into Eq. (2), and using the relation between vectors **a** and **b**, the following governing equation is obtained:

$$\left[\mathbf{Q} + s\left(\mathbf{R} - \mathbf{R}^T\right) + s^2\mathbf{T}\right]\mathbf{a} = \mathbf{0}. \tag{14}$$

It is found that Eq. (14), called the pseudo-Stroh formalism [38], includes eight eigenvalues s and four pairs of opposite numbers.

Using Eq. (11), Eq. (14) is then recast into an 8×8 linear eigensystem

$$\mathbf{N}\begin{bmatrix} \mathbf{a} \\ \mathbf{b} \end{bmatrix} = s\begin{bmatrix} \mathbf{a} \\ \mathbf{b} \end{bmatrix}, \tag{15}$$

where

$$\mathbf{N} = \begin{bmatrix} \mathbf{T}^{-1}\mathbf{R}^T & \mathbf{T}^{-1} \\ -\mathbf{Q} - \mathbf{R}\mathbf{T}^{-1}\mathbf{R}^T & \mathbf{R}\mathbf{T}^{-1} \end{bmatrix}. \tag{16}$$

We distinguish the corresponding eight eigenvectors by attaching a subscript to **a** and **b**. Then the general solution for the extended displacement and stress vectors is derived as

$$\begin{bmatrix} \mathbf{u} \\ \mathbf{t} \end{bmatrix} = \begin{bmatrix} \mathbf{A_1} & \mathbf{A_2} \\ \mathbf{B_1} & \mathbf{B_2} \end{bmatrix} \left\langle e^{s^* x_3} \right\rangle \begin{bmatrix} \mathbf{K_1} \\ \mathbf{K_2} \end{bmatrix}, \tag{17}$$

where

$$\begin{aligned} &\mathbf{A}_1 = [\boldsymbol{a}_1,\ \boldsymbol{a}_2,\ \boldsymbol{a}_3,\ \boldsymbol{a}_4],\ \mathbf{A}_2 = [\boldsymbol{a}_5,\ \boldsymbol{a}_6,\ \boldsymbol{a}_7,\ \boldsymbol{a}_8], \\ &\mathbf{B}_1 = [\boldsymbol{b}_1,\ \boldsymbol{b}_2,\ \boldsymbol{b}_3,\ \boldsymbol{b}_4],\ \mathbf{B}_2 = [\boldsymbol{b}_5,\ \boldsymbol{b}_6,\ \boldsymbol{b}_7,\ \boldsymbol{b}_8], \\ &\left\langle e^{s^* x_3} \right\rangle = \mathrm{diag}\left[e^{s_1 x_3},\ e^{s_2 x_3},\ \ldots,\ e^{s_8 x_3}\right]. \end{aligned} \tag{18}$$

Both $\mathbf{K}_1$ and $\mathbf{K}_2$ are 4×1 vectors to be determined by the external loads on the surfaces of plates, diag[] is a diagonal matrix.

According to the boundary condition at the bottom surface of plate, we can obtain the constant vectors $\mathbf{K}_1$ and $\mathbf{K}_2$ and substituting them into Eq. (17), the general solutions of the extended displacement and stress become

$$\begin{bmatrix} \mathbf{u}(x_3) \\ \mathbf{t}(x_3) \end{bmatrix} = \mathbf{P}_j(x_3) \begin{bmatrix} \mathbf{u}\left(x_{3-}^{(j)}\right) \\ \mathbf{t}\left(x_{3-}^{(j)}\right) \end{bmatrix}, \tag{19}$$

where $\mathbf{P}_j(x_3)$ is the propagator matrix of layer j, and $x_{3-}^{(j)} \le x_3 \le x_{3+}^{(j)}$, i.e.,

$$\mathbf{P}_j(x_3) = \begin{bmatrix} \mathbf{A_1} & \mathbf{A_2} \\ \mathbf{B_1} & \mathbf{B_2} \end{bmatrix} \left\langle e^{s^*(x_3 - x_{3-}^{(j)})} \right\rangle \begin{bmatrix} \mathbf{A_1} & \mathbf{A_2} \\ \mathbf{B_1} & \mathbf{B_2} \end{bmatrix}^{-1}. \tag{20}$$

Using the imperfect boundary conditions (5) at partial interfaces, the propagator relation from $x_3 = 0$ to $x_3 = H$ of QC layered plate is derived as

$$\begin{bmatrix} \mathbf{u}(H) \\ \mathbf{t}(H) \end{bmatrix} = \mathbf{Y} \begin{bmatrix} \mathbf{u}(0) \\ \mathbf{t}(0) \end{bmatrix}, \tag{21}$$

where the propagator matrix $\mathbf{Y}$ is defined as

$$\mathbf{Y} = \mathbf{P}_N(h_N)\mathbf{M}_{N-1}\mathbf{P}_{N-1}(h_{N-1})\mathbf{M}_{N-2}\cdots\mathbf{P}_2(h_2)\mathbf{M}_1\mathbf{P}_1(h_1), \tag{22}$$

where $\mathbf{M}_j$ ($j = 1, 2, \ldots, N$–1) are the propagator matrices of imperfect interfaces and $\mathbf{P}_j$ ($j = 1, 2, \ldots, N$) are seen in Eq. (20). When $R_i^{(j)} = 0$, all $\mathbf{M}_j$ become identity matrices in Eq. (22). Thus, Eq. (21) is completely consistent with the results of perfect case [12].

3.1 Static deformation

In this section, the general solution of static deformation for a simply-supported multilayered 1D QC plate with imperfect interfaces is presented. The general solution of the extended displacement and stress of layered plate can be solved by omitting the time-dependent terms, i.e., $\omega = 0$.

If the top surface of plate is only subjected to the phonon mechanical loads and the bottom surface is free of traction, the boundary conditions are

$$\mathbf{t}(H) = [0,\ 0,\ \sigma_0 \sin px_1 \sin qx_2,\ 0]^T, \quad \mathbf{t}(0) = [0,\ 0,\ 0,\ 0]^T. \tag{23}$$

Thus, Eq. (21) becomes

$$\begin{bmatrix} \mathbf{u}(H) \\ \mathbf{t}(H) \end{bmatrix} = \begin{bmatrix} \mathbf{C}_{11} & \mathbf{C}_{12} \\ \mathbf{C}_{21} & \mathbf{C}_{22} \end{bmatrix} \begin{bmatrix} \mathbf{u}(0) \\ \mathbf{0} \end{bmatrix}, \tag{24}$$

where $\mathbf{C}_{ij}$ is the submatrices of $\mathbf{Y}$ in Eq. (22). Substituting Eq. (23) in Eq. (24), the unknown displacements at the bottom and top surfaces are obtained as

$$\mathbf{u}(0) = \mathbf{C}_{21}^{-1}\mathbf{t}(H), \quad \mathbf{u}(H) = \mathbf{C}_{11}\mathbf{C}_{21}^{-1}\mathbf{t}(H). \tag{25}$$

Finally, the extended displacements and extended stresses at any position of 1D hexagonal QC layered plates with imperfect interfaces can be obtained as

$$\begin{bmatrix} \mathbf{u}(x_3^{(j)}) \\ \mathbf{t}(x_3^{(j)}) \end{bmatrix} = \mathbf{P}_j(x_3^{(j)} - x_{3-}^{(j)})\mathbf{M}_{j-1}\mathbf{P}_{j-1}(h_{j-1})\mathbf{M}_{j-2}\cdots\mathbf{P}_2(h_2)\mathbf{M}_1\mathbf{P}_1(h_1)\begin{bmatrix} \mathbf{u}(0) \\ \mathbf{0} \end{bmatrix}. \tag{26}$$

3.2 Free vibration

For free vibration analysis, both the top and bottom surfaces of the plate are traction-free, then Eq. (21) is simplified as

$$\begin{bmatrix} \mathbf{u}(H) \\ \mathbf{0} \end{bmatrix} = \begin{bmatrix} \mathbf{C}_{11} & \mathbf{C}_{12} \\ \mathbf{C}_{21} & \mathbf{C}_{22} \end{bmatrix}\begin{bmatrix} \mathbf{u}(0) \\ \mathbf{0} \end{bmatrix}. \tag{27}$$

There are non-zero solutions in Eq. (27), and the submatrix $\mathbf{C}_{21}$ must satisfy

$$\det[\mathbf{C}_{21}] = 0, \tag{28}$$

where det[] denotes the determinant of a matrix.

3.3 Forced vibration

In this section, the response of 1D hexagonal QC layered plate is considered subject to a harmonic excitation on the top surface, i.e.,

$$\mathbf{t}(H) = [0,\ 0,\ \sigma_0 \mathrm{e}^{\mathrm{i}\omega t}\sin px_1 \sin qx_2,\ 0]^T, \quad \mathbf{t}(0) = [0,\ 0,\ 0,\ 0]^T. \tag{29}$$

Substituting Eq. (29) into Eq. (21), the unknown displacement vectors at the top and bottom surfaces can be derived as

$$\mathbf{u}(0) = \mathbf{C}_{21}^{-1}\mathbf{t}(H), \quad \mathbf{u}(H) = \mathbf{C}_{11}\mathbf{C}_{21}^{-1}\mathbf{t}(H). \tag{30}$$

4 Numerical examples

In the numerical analysis, we consider two sandwich C/QC/C and QC/C/QC plates made up of Al–Ni–Co (QC) and $BaTiO_3$ (C) materials, where the material properties of these two materials are listed in Table 1. Each adjacent two layers of plates are imperfect bonding. Referring to the previous work [12, 13, 28, 38], the dimension of the plate is taken as $L_1 \times L_2 \times H = 1 \times 1 \times 0.3$ m and three layers have equal thickness of 0.1 m. In general, an interface can be modeled as a thin layer with certain material properties in which displacements and stresses are discontinuous across the interface layer [39]. As an extreme case, the spring model without any thickness of interface layer allows a jump of displacements but continuous stresses across the interface. Liu et al. [40, 41] introduced several imperfect interface models including the direct thin-layer, spring and density models to investigate the effect of these models on the response of the layered half-space under time-harmonic surface loadings and found that under either vertical or horizontal load, the thin-layer model with a very small thickness predicts nearly the same result as that by the spring model without any thickness. Thus, the thickness of interface layers is neglected in our analysis. Furthermore, we assume $R_3^{(j)} = 0$ to avoid material embeddedness that is physically impossible, and also assume $R_1^{(j)} = R_2^{(j)} = R_4^{(j)} = R^{(j)}$, where $R^{(j)}$ denotes the imperfect interface parameter at the j-th interface.

Table 1 Material properties of QC [42] and C [43] materials (C_{ij}, K_i and R_i in 10^9 N/m^2 and ρ in 10^3 kg/m^3)

	$C_{11}=C_{22}$	C_{12}	$C_{13}=C_{23}$	C_{33}	$C_{44}=C_{55}$	C_{66}
QC	234.33	57.41	66.63	232.21	70.19	88.46
C	166	77	78	162	43	44.5
	K_1	K_2	R_1	R_2	R_3	ρ
QC	122	24	8.846	8.846	8.846	4.186
C	–	–	–	–	–	5.8

4.1 Effect of imperfect interface on static deformation

We assume that the imperfect degree at two imperfect interfaces is the same, i.e., $R^{(1)}=R^{(2)}=R^{(\mathrm{Im})}$. It is assumed that the mechanical loads of phonon field act on the top surface of two sandwich plates, i.e., $\sigma_0=1$ N/m^2 ($m=n=1$). The responses at $(x_1, x_2)=(0.75L_1, 0.25L_2)$ are discussed in the numerical analysis.

Figure 2 shows the effect of imperfect interface parameter $R^{(\mathrm{Im})}$ on the phonon displacements, phason displacement of two sandwich plates. It can be observed that the phonon and phason displacements on the top and bottom surfaces of two sandwich plates always increase with increasing $R^{(\mathrm{Im})}$. The phonon displacement u_1 jumps across the imperfect interfaces. When $R^{(\mathrm{Im})}=0$, it corresponds to the perfect interface case, which agrees well with the previous results [12]. The stacking sequence has a great influence on the phason displacement.

Figure 3 plots the effect of $R^{(\mathrm{Im})}$ on the phonon stresses and phason stress of two sandwich plates. It can be found that the imperfect interface parameter has a large influence on the phonon stresses of the middle layer. It is interesting to further note that increasing $R^{(\mathrm{Im})}$ can reduce the shear stress σ_{13} at the interfaces, which can provide a way for defect optimization and help us introduce the imperfect interface to reduce stress. The phason stress H_{33} in QC plate is greatly affected by the imperfect interface parameter.

Table 2 lists the phonon displacements for two sandwich plates with different $R^{(\mathrm{Im})}$ between the layers for the point $(x_1, x_2)=(0.75L_1, 0.25L_2)$ at the bottom of plate. It can be observed that the magnitude of phonon displacements of two sandwich plates always increases with increasing $R^{(\mathrm{Im})}$. The phonon displacement of QC/C/QC plate is smaller than that of C/QC/C plate. When the imperfect interface parameter of upper or lower interface becomes small, the phonon displacement u_3 of two sandwich plates always decreases, however, the phonon displacement u_1 of two sandwich plates displays a different trend.

4.2 Effect of imperfect interface on free vibration

In this section, the effects of different $R^{(\mathrm{Im})}$ on the natural frequencies of two sandwich plates are analyzed. Since the lowest frequencies are of most importance in free vibration of any system, the fixed values $m=n=1$ are selected and the first four natural frequencies of two sandwich plates are listed in Table 3. The natural frequencies are normalized as

$$\Omega=\omega L_1\Big/\sqrt{C_{\max}/\rho_{\max}}, \tag{31}$$

where $C_{\max}$ and $\rho_{\max}$ represent the maximum value of phonon elastic constant and density in the entire plate, respectively. From Table 3, it can be obviously seen that the natural frequencies of two sandwich plates always increase with increasing mode while they decrease with increasing $R^{(\mathrm{Im})}$ of two imperfect interfaces. It is interesting to note that the decrease $R^{(\mathrm{Im})}$ of upper or lower interface results in an increase of the natural frequency of two sandwich plates. The natural frequency of sandwich C/QC/C plate is greatly dependent on the lower interface while the natural frequency of sandwich QC/C/QC plate greatly depends on the upper interface. Therefore, the vibrational characteristics of two sandwich plates can be optimized by imposing imperfect interfaces and controlling the stacking sequence artificially.

4.3 Effect of imperfect interface on forced vibration

In this section, to investigate the forced vibration response of two sandwich plates, the top surface of plate is subjected to a harmonic excitation. We assumed that the amplitude $\sigma_0=1$ N/m^2 and the normalized input

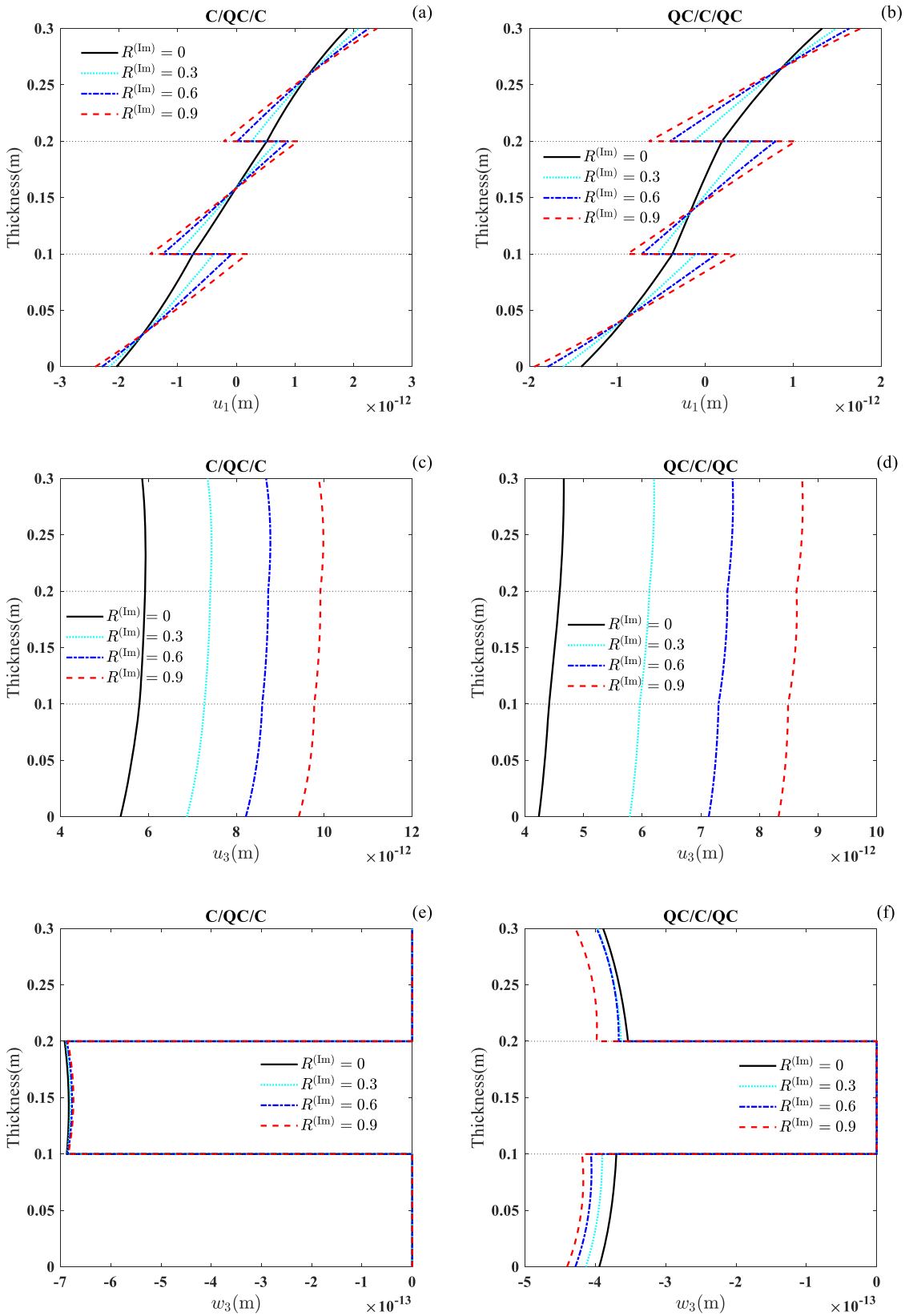

Fig. 2 Variation of phonon and phason displacements of two sandwich plates along the thickness direction

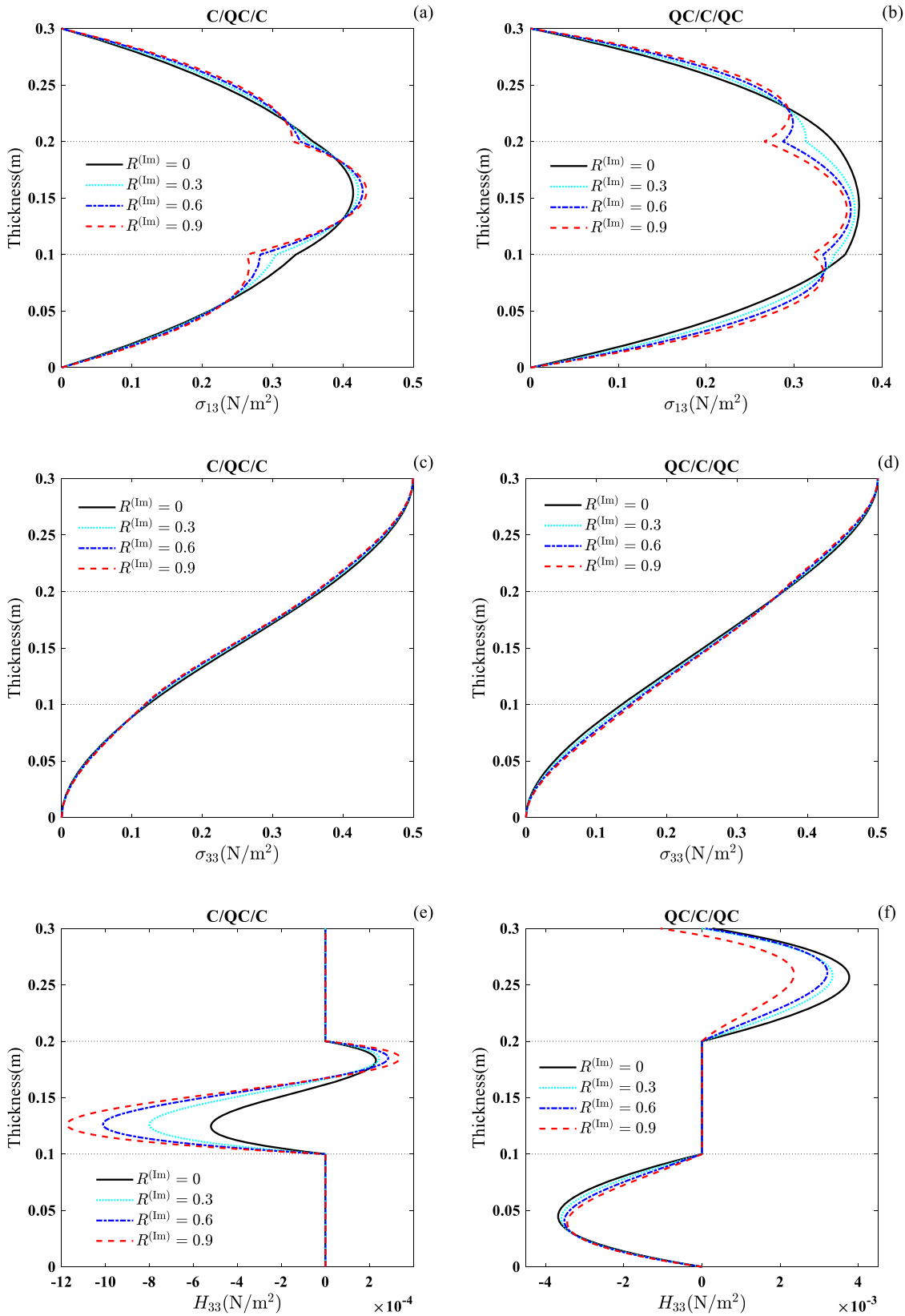

Fig. 3 Variation of phonon and phason stresses of two sandwich plates along the thickness direction

Table 2 Phonon displacements of two sandwich plates with imperfect interfaces (u_i in 10^{-12} m)

$R^{(\mathrm{Im})}$		$R^{(1)} = R^{(2)} = R^{(\mathrm{Im})}$				$2R^{(1)} = R^{(2)} = R^{(\mathrm{Im})}$			$R^{(1)} = 2R^{(2)} = R^{(\mathrm{Im})}$		
		0 [12]	0.3	0.6	0.9	0.3	0.6	0.9	0.3	0.6	0.9
C/QC/C	$u_1 = u_2$	–2.045948	–2.172075	–2.293229	–2.407790	–2.178692	–2.298637	–2.407971	–2.101048	–2.161017	–2.222979
	u_3	5.364998	6.874114	8.215567	9.420701	6.431213	7.419211	8.337690	6.568209	7.614145	8.543904
QC/C/QC	$u_1 = u_2$	–1.410641	–1.617650	–1.793140	–1.944784	–1.601323	–1.758825	–1.892506	–1.533414	–1.646786	–1.751746
	u_3	4.234812	5.783985	7.133658	8.323947	5.475697	6.540970	7.475774	5.332205	6.334024	7.252665

Table 3 Normalized natural frequencies Ω of two sandwich plates

	Ω	$R^{(1)} = R^{(2)} = R^{(\mathrm{Im})}$				$2R^{(1)} = R^{(2)} = R^{(\mathrm{Im})}$			$R^{(1)} = 2R^{(2)} = R^{(\mathrm{Im})}$		
		0 [13]	0.3	0.6	0.9	0.3	0.6	0.9	0.3	0.6	0.9
C/QC/C	1	1.093018	0.991928	0.920514	0.867264	1.019021	0.961179	0.914763	1.010310	0.950486	0.904763
	2	2.332373	2.314666	2.297858	2.281959	2.320095	2.308279	2.296951	2.317781	2.303425	2.289392
	3	3.764697	3.716734	3.528725	3.200881	3.731130	3.700662	3.502214	3.724324	3.686160	3.361540
	4	5.508447	4.116503	3.674545	3.637655	4.412400	3.848406	3.673054	4.271072	3.693318	3.650730
QC/C/QC	1	1.346240	1.173859	1.066191	0.991621	1.202956	1.109109	1.042243	1.217595	1.126404	1.058064
	2	2.751514	2.728747	2.705660	2.682488	2.733337	2.715984	2.697898	2.735808	2.719861	2.703865
	3	4.256689	4.183797	4.113207	4.046918	4.199275	4.145896	4.096579	4.205993	4.155583	4.106365
	4	6.422412	5.209753	4.648465	4.330957	5.321619	4.743660	4.404617	5.489958	4.969695	4.642595

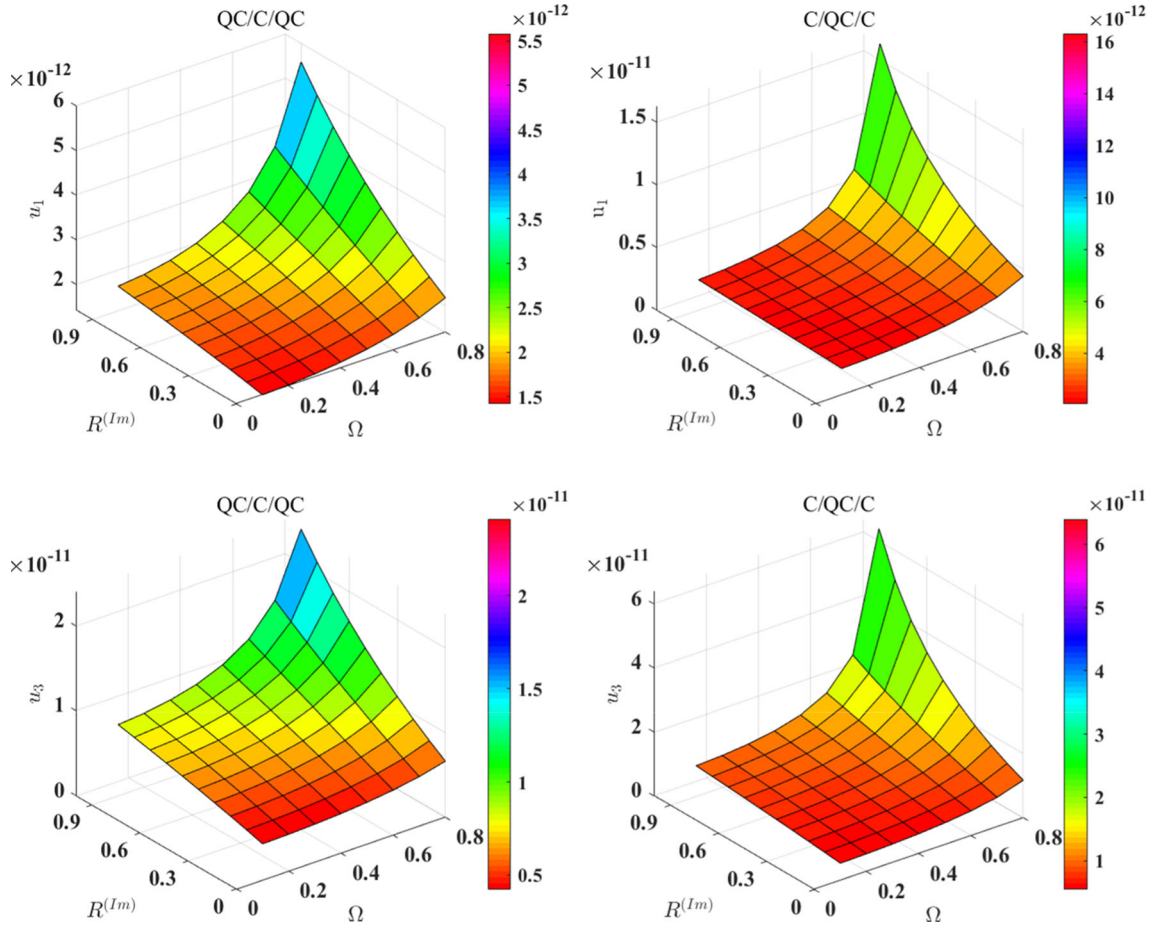

Fig. 4 Effect of input frequency on phonon displacements u_1, u_3 of two sandwich C/QC/C and QC/C/QC plates with different $R^{(\mathrm{Im})}$

frequencies Ω = 0.1, 0.2, …, 0.8, are smaller than the first natural frequency of vibration to avoid resonance. The forced vibration responses of two C/QC/C and QC/C/QC sandwich plates are considered below.

Figure 4 illustrates the variation of phonon displacements of two sandwich C/QC/C and QC/C/QC plates with harmonic excitation and imperfect interface parameter $R^{(\mathrm{Im})}$. The results show that the phonon displacements of two sandwich plates always increase with increasing $R^{(\mathrm{Im})}$ and forcing frequency. It can be further seen that the C/QC/C sandwich plate is more sensitive to imperfect interfaces in forced vibration, which indicates the stiffness of sandwich QC/C/QC plate is higher than that of sandwich C/QC/C plate. This also confirms that QC materials are suitable for the surface coatings of new composites in engineering practice.

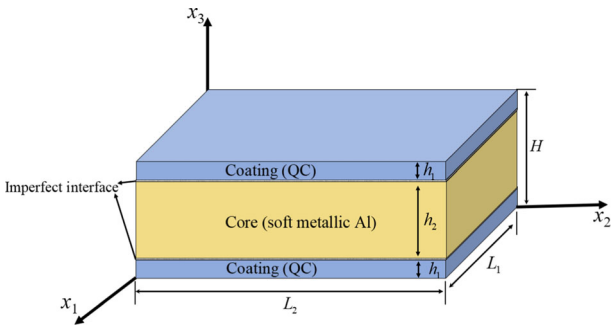

Fig. 5 A QC-coated Al-based composite plate with imperfect interfaces

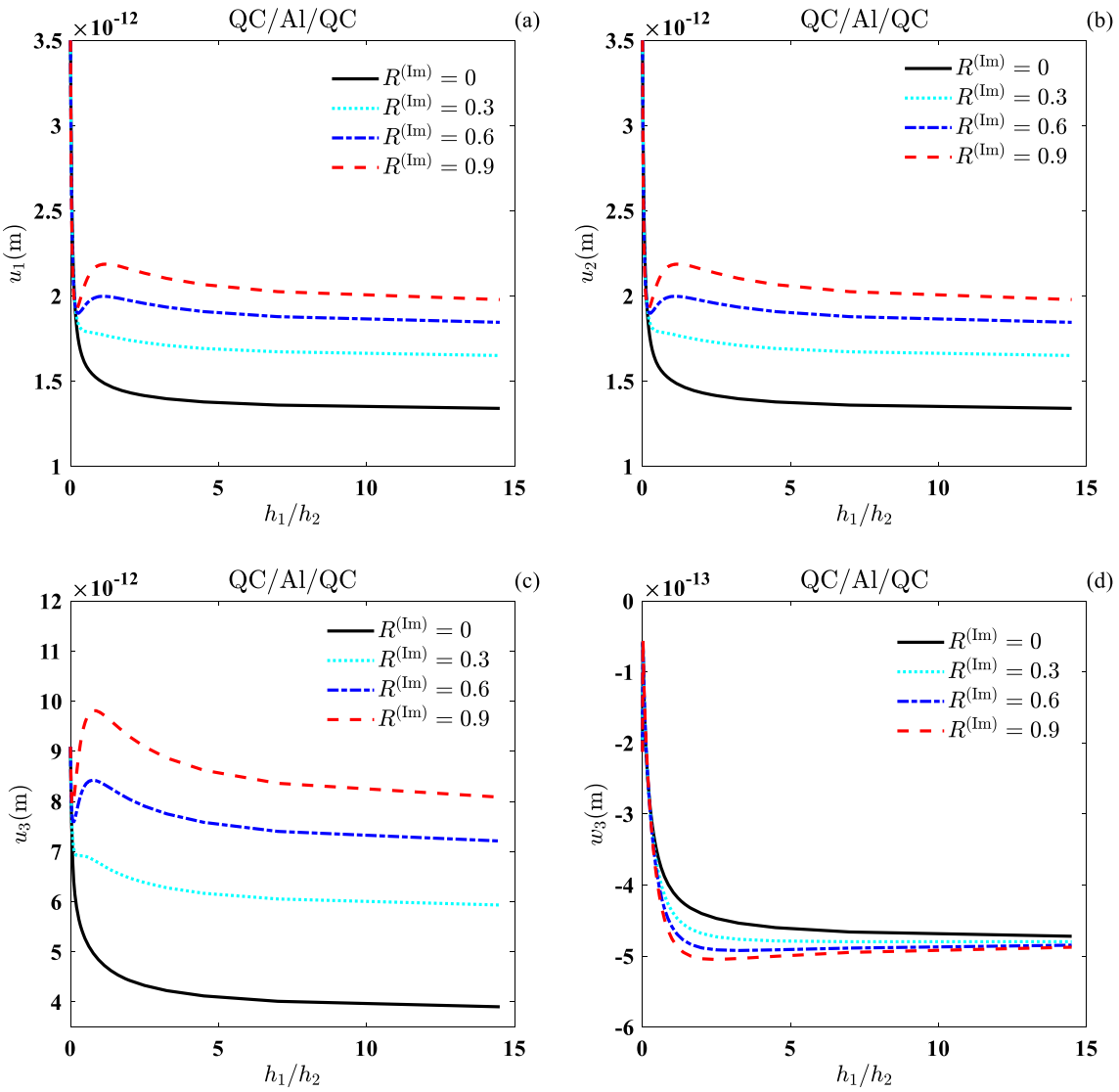

Fig. 6 Variation of phonon and phason displacements with thickness ratio of QC coatings and core material Al in QC/Al/QC plate for different $R^{(\mathrm{Im})}$

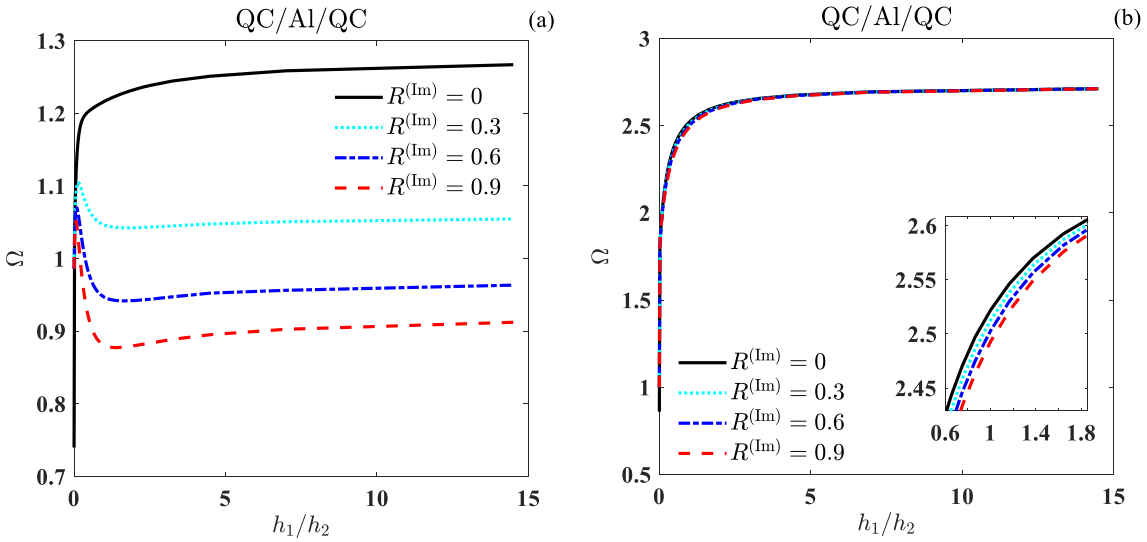

Fig. 7 Variation of the first two order normalized natural frequency Ω with thickness ratio of QC coatings and core material Al in QC/Al/QC plate for different $R^{(\mathrm{Im})}$

4.4 Application of the present 3D plate model to QC coated Al-based composites

Due to their brittle at room temperature, QCs are difficult to be used directly as structural parts, but they can be commonly used as hard and abrasion-resistant coatings on softer metals or surface modification of soft metallic materials [44]. Duguet et al. [7] demonstrated the possibility of using complex metallic surface alloys as interface layers to enhance the adhesion between QCs and simple metal substrates. By using the thermal spraying technology, QC coatings and QC-reinforced composites can be produced [45]. From the experimental point of view, the interfacial reaction between Al matrix and QC reinforcing particles was considered to enhance the strength of the Al/QC composites [9]. By ductile vanadium layers and brittle Al-Cu-Fe-based QC layers, the multilayered coatings were formed and the annealed multilayered structure showed a high flow stress due to QC strengthening [8]. To reveal the mechanical behavior of QC coated Al-based composites in engineering practice, we consider the effect of thickness of QC coatings and imperfect interface parameter on bending deformation and vibrational response of QC coated Al-based composites (i.e., QC/Al/QC plate) based on the present 3D layered plate model.

As shown in Fig. 5, h_1 and h_2 denote the thickness of QC coatings and core material Al, respectively, and H $(= 2h_1 + h_2)$ denotes the total thickness of QC/Al/QC plate. The material properties of QC are listed in Table 1 and the material properties of metallic Al [46] are $C_{11} = C_{22} = C_{33} = 108.2 \times 10^9$ N/m^2, $C_{12} = C_{13} = C_{23} = 61.3 \times 10^9$ N/m^2, $C_{44} = C_{55} = C_{66} = 28.5 \times 10^9$ N/m^2 and $\rho = 2699$ kg/m^3.

Figure 6 shows the variation of phonon and phason displacements with thickness ratio h_1/h_2 of QC coatings and core material Al in QC/Al/QC plate for different imperfect interface parameters ($R^{(\mathrm{Im})} = 0$, 0.3, 0.6, 0.9) under surface loading $\sigma_0 = 1$ N/m^2. It is interesting to note that in general, the phonon displacements decrease with increasing h_1/h_2 for both perfect and imperfect interfaces, while the magnitude of phason displacement increases with increasing h_1/h_2 for both perfect and imperfect interfaces. It indicates that an increase in the thickness of QC coatings can greatly enhance the stiffness of sandwich plate as compared to pure Al plate. However, the imperfect interfaces can reduce the stiffness of the plate.

Figure 7 shows the variation of the first two order normalized natural frequency with h_1/h_2 of QC/Al/QC plate for different $R^{(\mathrm{Im})}$ under free vibration. It can be seen that with increasing thickness of QC coatings, the first order normalized natural frequency always increases for the perfect interfaces, but the first order normalized natural frequency decreases first and then increases for the case of imperfect interfaces. However, the second order normalized natural frequency always increases with increasing thickness of QC coatings for both perfect and imperfect interfaces.

Figure 8 plots the effect of both h_1/h_2 and $R^{(\mathrm{Im})}$ on phonon displacements u_1, u_3 and phason displacement w_3 of QC/Al/QC plate under the forcing frequencies $\Omega = 0.4$ (see Fig. 8a–c) and $\Omega = 0.6$ (see Fig. 8d–f). It can be observed that the phonon displacements u_1 and u_3 reach their minimum values for QC plate with perfect

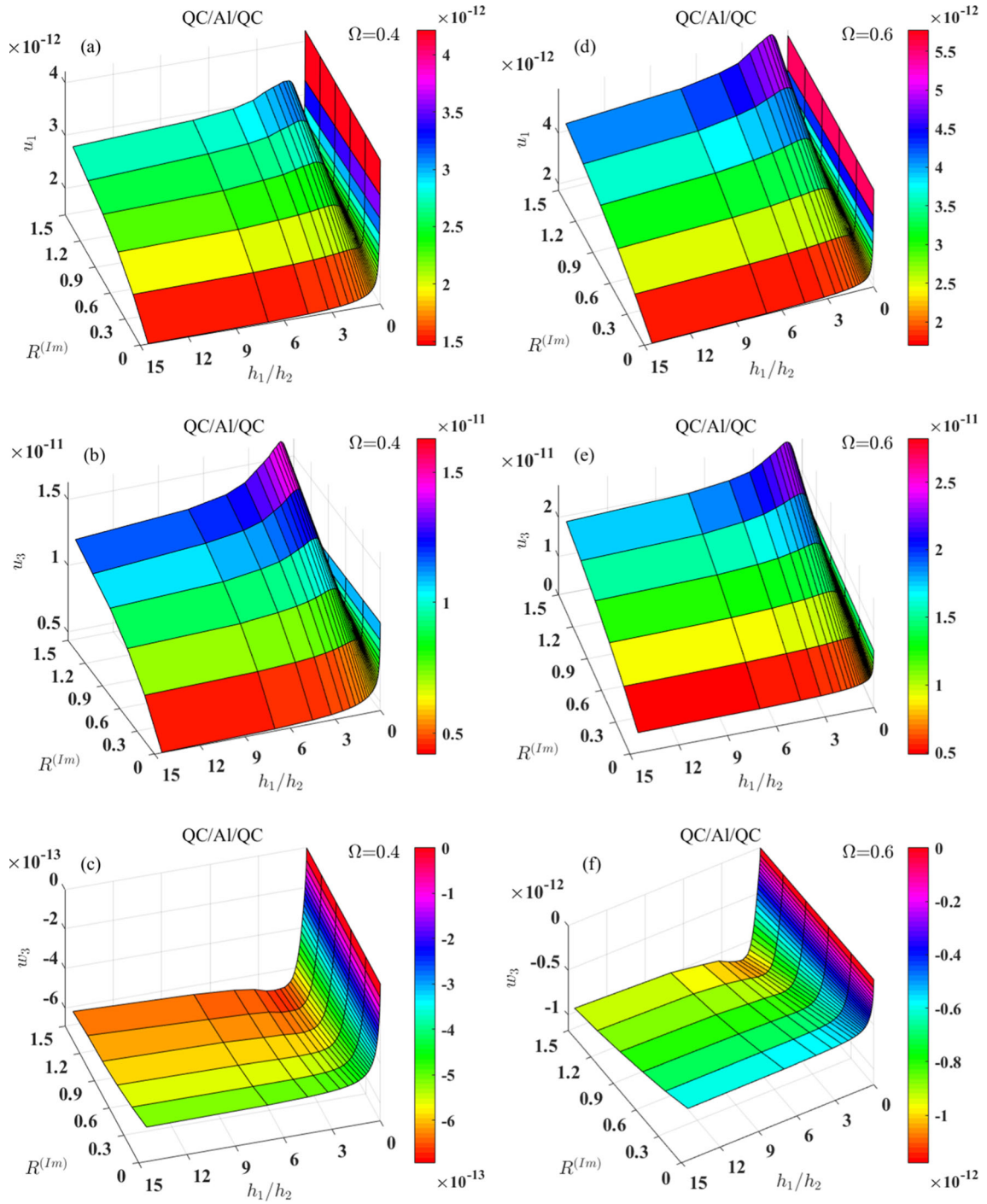

Fig. 8 Effect of both h_1/h_2 and $R^{(\mathrm{Im})}$ on phonon displacements u_1, u_3 and phason displacement w_3 of QC/Al/QC plate under the forcing frequencies $\Omega = 0.4$ and $\Omega = 0.6$

bonding. Besides, the phonon displacement u_1 reaches its peak for pure Al plate, while the phonon displacement u_3 reaches its peak at about $h_1/h_2 = 1$ for QC/Al/QC plate with imperfect interfaces. Furthermore, the phason displacement w_3 displays a different trend from the phonon displacements due to the special structures of QCs.

5 Conclusions and outlook

The static deformation and vibrational response of 1D hexagonal QC layered plate with imperfect interfaces are investigated in this work and exact solutions of the extended displacement and stress of 1D hexagonal QC layered plate with imperfect interfaces are derived by using the propagation matrix method and pseudo-Stroh formalism. Numerical examples are provided to show the effects of imperfect interface parameter and stacking sequence on the static deformation and vibrational response of two sandwich plates. Some useful conclusions can be drawn:

(i) An increase of the imperfect interface parameter can reduce the shear phonon stress at the interfaces in the bending of QC layered plates with imperfect interfaces. When the imperfect interface parameter of the upper or lower interface becomes small, the phonon displacement u_3 of two sandwich plates always decreases, however, the phonon displacement u_1 of two sandwich plates displays a different trend.
(ii) The natural frequencies of two sandwich plates always decrease with increasing imperfect interface parameter. The decrease of imperfect interface parameter of upper or lower interface results in an increase in the natural frequency of two sandwich plates.
(iii) The displacements of phonon and phason fields of two sandwich plates always increase with increasing both imperfect interface parameter and input frequency. In forced vibration, the sandwich C/QC/C plate is more sensitive to imperfect interfaces than the sandwich QC/C/QC plate.
(iv) An increase in the thickness of QC coatings can greatly enhance the stiffness of the sandwich plate as compared to the pure Al plate. Thus, QCs are suitable for surface coatings on soft metallic materials in engineering practice.

However, the present study mainly focuses on simply supported boundary conditions at four sides of plate, the analytical method, the phonon-phason couplings and the classical elasticity theory. In the next step, arbitrary boundary conditions, experimental research, various numerical methods such as the molecular dynamics simulation, the finite element method, the differential quadrature approach, the meshless method, etc., the multi-field couplings among phonon, phason, thermal and electric fields, and the size-dependent effect at small scale will be key issues in the further study.

Acknowledgements Project supported by the National Natural Science Foundation of China (Nos. 12072166 and 11862021), Program for Science and Technology of Inner Mongolia Autonomous Region (No. 2021GG0254), the Natural Science Foundation of Inner Mongolia Autonomous Region of China (2020MS01006) and the Independent Research Key Program of Center for Applied Mathematics of Inner Mongolia (ZZYJZD2022002).

References

1. Fan, T.Y.: Mathematical theory of elasticity and defects of quasicrystals. Adv Mech **30**(2), 161–174 (2000). https://doi.org/10.3321/j.issn:1000-0992.2000.02.001(inChinese)
2. Fan, T.Y.: Mathematical theory of elasticity of quasicrystals and its applications. Science Press. (2011)
3. Stadnik, Z.M.: Physical Properties of Quasicrystals. Springer, Berlin Heidelberg (1999)
4. Guo, X., Chen, J., Yu, H., Liao, H., Coddet, C.: A study on the microstructure and tribological behavior of cold-sprayed metal matrix composites reinforced by particulate quasicrystal. Surf. Coat. Technol. **268**, 94–98 (2015). https://doi.org/10.1016/j.surfcoat.2014.05.062
5. Zhang, J.S., Pei, L.X., Du, H.W., Liang, W., Xu, C.X., Lu, B.F.: Effect of Mg-based spherical quasicrystals on microstructure and mechanical properties of AZ91 alloys. J. Alloy. Compd. **453**(1), 309–315 (2006)
6. Louzguine-Luzgin, D.V., Inoue, A.: Formation and properties of quasicrystals. Annu. Rev. Mater. Res. **38**, 403–423 (2008)
7. Duguet, T., Ledieu, J., Dubois, J.M., Fournée, V.: Surface alloys as interfacial layers between quasicrystalline and periodic materials. Journal of Physics: Condensed Matter. **20**(31) (2008). Doi: https://doi.org/10.1088/0953-8984/20/31/314009
8. Chang, S.Y., Chen, B.J., Hsiao, Y.T., Wang, D.S., et al.: Preparation and nanoscopic plastic deformation of toughened Al-Cu-Fe-based quasicrystal/vanadium multilayered coatings. Mater. Chem. Phys. **213**, 277–284 (2018)
9. Ali, F., Scudino, S., Anwar, M.S., Shahid, R.N., et al.: Al-based metal matrix composites reinforced with Al–Cu–Fe quasicrystalline particles: Strengthening by interfacial reaction. J. Alloy. Compd. **607**, 274279 (2014). https://doi.org/10.1016/j.jallcom.2014.04.086
10. Wei, D., He, Z.: Multilayered sandwich-like architecture containing large-scale faceted Al–Cu–Fe quasicrystal grains. Mater. Charact. **111**, 154–161 (2016). https://doi.org/10.1016/j.matchar.2015.11.027

11. Yang, L.Z., Gao, Y., Pan, E., Waksmanski, N.: An exact solution for a multilayered two-dimensional decagonal quasicrystal plate. Int. J. Solids Struct. **51**(9), 1737–1749 (2014)
12. Yang, L.Z., Gao, Y., Pan, E., Waksmanski, N.: An exact closed-form solution for a multilayered one-dimensional orthorhombic quasicrystal plate. Acta Mech. **226**(11), 3611–3621 (2015)
13. Waksmanski, N., Pan, E., Yang, L.Z., Gao, Y.: Free vibration of a multilayered one-dimensional quasi-crystal plate. Journal of Vibration and Acoustics.**136**(4) (2014)
14. Pan, E., Waksmanski, N.: Nonlocal analytical solutions for multilayered one-dimensional quasicrystal nanoplates. Journal of Vibration and Acoustics. **139**(2) (2017)
15. Li, X.F., Guo, J.H., Sun, T.Y.: Bending deformation of multilayered one-dimensional quasicrystal nanoplates based on the modified couple stress theory. Acta Mech. Solida Sin. **32**(6), 785–802 (2019). https://doi.org/10.1007/s10338-019-00120-8
16. Guo, J.H., Zhang, M. Chen, W.Q., Zhang, X.Y.: Free and forced vibration of layered one-dimensional quasicrystal nanoplates with modified couple-stresseffect. Science China (Physics, Mechanics and Astronomy). **63**(07), 124–125 (2020). Doi: https://doi.org/10.1007/s11433-020-1547-3
17. Zhang, L., Guo, J.H., Xing, Y.M.: Bending analysis of functionally graded one-dimensional hexagonal piezoelectric quasicrystal multilayered simply supported nanoplates based on nonlocal strain gradient theory. Acta Mech. Solida Sin. **34**(2), 15 (2021)
18. Sun, T.Y., Guo, J.H.: Free vibration and bending of one-dimensional quasicrystal layered composite beams by using the state space and differential quadrature approach. Acta Mech. (2022). https://doi.org/10.1007/s00707-022-03270-y
19. Cheng, Z.Q., Jemah, A.K., Williams, F.W.: Theory for multilayered anisotropic plates with weakened interfaces. J. Appl. Mech. **63**, 1019–1026 (1996). https://doi.org/10.1115/1.2787221
20. Cheng, Z.Q., He, L.H., Kitipornchai, S.: Influence of imperfect interfaces on bending and vibration of laminated composite shells. Int. J. Solids Struct. **37**(15), 2127–2150 (2000)
21. Fan, H., Sze, K.Y.: A micro-mechanics model for imperfect interface in dielectric materials. Mechanics of Materials. **33**(6), 363–370 (2001). Doi: https://doi.org/10.1016/S0167-6636(01)00053-9
22. Bui, V.: Imperfect interlaminar interfaces in laminated composites: bending, buckling and transient reponses. Compos. Sci. Technol. **59**(15), 2269–2277 (1999). https://doi.org/10.1016/S0266-3538(99)00081-0
23. Chen, W.Q., Cai, J.B., Ye, G.R.: Exact solutions of cross-ply laminates with bonding imperfections. AIAA J. **41**(11), 2244–2250 (2003)
24. Chen, W.Q., Kang, Y.L.: Three-dimensional exact analysis of angle-ply laminates in cylindrical bending with interfacial damage via state-space method. Compos. Struct. **64**(3/4), 275–283 (2004)
25. Wang, X., Pan, E.: Exact solutions for simply supported and multilayered piezothermoelastic plates with imperfect interfaces. Open Mech J. **1**(1), 1–10 (2007)
26. Chen, W.Q., Zhou, Y.Y., Lü, C.F., Ding, H.J.: Bending of multiferroic laminated rectangular plates with imperfect interlaminar bonding. Eur. J Mech A Solids **28**(4), 720–727 (2009). https://doi.org/10.1016/j.euromechsol.2009.02.008
27. Kuo, H.Y., Huang, C.S., Pan, E.: Effect of imperfect interfaces on the field response of multilayered magneto-electro-elastic composites under surface loading. Smart Materials and Structures. **28**(11), 115006 (2019)
28. Vattré, A., Pan, E.: Thermoelasticity of multilayered plates with imperfect interfaces. International Journal of Engineering Science. **158** (2021)
29. López, J.C., Realpozo, R.A., Rodríguez-Ramos, J., Quintero, R.H.: Behavior of piezoelectric layered composites with mechanical and electrical non-uniform imperfect contacts. Meccanica **55**(1), 125–138 (2020)
30. Li, J.P., Zhang, L.: High-precision calculation of electromagnetic scattering by the Burton-Miller type regularized method of moments. Eng. Anal. Boundary Elem. **133**, 177–184 (2021)
31. Li, J.P., Gu, Y., Qin, Q.H., Zhang, L.: The rapid assessment for three-dimensional potential model of large-scale particle system by a modified multilevel fast multipole algorithm. Computers and Mathematics with Applications. **89** (2021)
32. Li, J.P., Zhang, L., Qin, Q.H.: A regularized method of moments for three-dimensional time-harmonic electromagnetic scattering. Appl. Math. Lett. **112**, 106746 (2021)
33. Cheng, Z.Q., Kennedy, D., Williams, F.W.: Effect of Interfacial imperfection on buckling and bending behavior of composite laminates. AIAA J. **34**(12), 2590–2595 (1996). https://doi.org/10.2514/3.13443
34. Benveniste, Y.: A general interface model for a three-dimensional curved thin anisotropic interphase between two anisotropic media. J. Mech. Phys. Solids **54**(4), 708734 (2006). https://doi.org/10.1016/j.jmps.2005.10.009
35. Benveniste, Y.: Exact results for the local fields and the effective moduli of fibrous composites with thickly coated fibers. Journal of the Mechanics and Physics of Solids. **71**(nov.), 219–238 (2014). Doi: https://doi.org/10.1016/j.jmps.2014.07.005
36. Chen, T., Chiu, M.S., Weng, C.N.: Derivation of the generalized Young-Laplace equation of curved interfaces in nanoscaled solids. J. Appl. Phys. **100**(7), 65 (2006). https://doi.org/10.1063/1.2356094
37. Wang, Z., Zhu, J., Jin, X.Y., Chen, W.Q., Zhang, C.: Effective moduli of ellipsoidal particle reinforced piezoelectric composites with imperfect interfaces. J. Mech. Phys. Solids **65**, 138–156 (2014)
38. Pan, E.: Exact solution for simply supported and multilayered magneto-electro-elastic plates. J. Appl. Mech. **68**(4), 608–618 (2001)
39. Xu, P.C., Datta, S.K.: Guided waves in a bonded plate: A parametric study. Journal of Applied Physics. **67**(11) (1990)
40. Liu, H., Pan, E., Cai, Y.C.: General surface loading over layered transversely isotropic pavements with imperfect interfaces. Advances in Engineering Software. **115** (2018)
41. Liu, H., Pan, E.: Time-harmonic loading over transversely isotropic and layered elastic half-spaces with imperfect interfaces. Soil Dyn. Earthq. Eng. **107**, 35–47 (2018)
42. Fan, T.Y.: Mathematical theory and methods of mechanics of quasicrystalline materials. Engineering **05**(4), 407–448 (2013). https://doi.org/10.4236/eng.2013.54053
43. Stroh, A.N.: Dislocations and cracks in anisotropic elasticity. Phil. Mag. **3**(30), 625–646 (1958)
44. Dubois, J.M., Kang, S.S., Massiani, Y.: Application of quasicrystalline alloys to surface coating of soft metals. J. Non-Cryst. Solids **153–154**, 443–445 (1993)

45. Kenzari, S., Bonina, D., Dubois, J., Fournée, V.: Quasicrystal–polymer composites for selective laser sintering technology. Mater. Des. **35**(Mar.), 691–695 (2012)
46. Pan, E., Chen, W.Q.: Static Green's Functions in Anisotropic Media. Cambridge University Press, Cambridge (2015)